19e Journées de l'Hydrodynamique
26 – 28 novembre 2024, Nantes

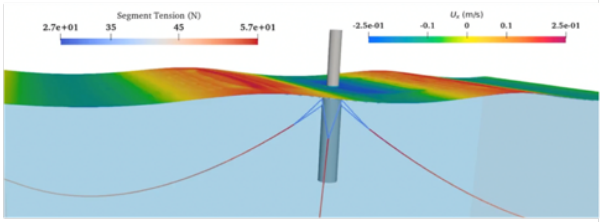

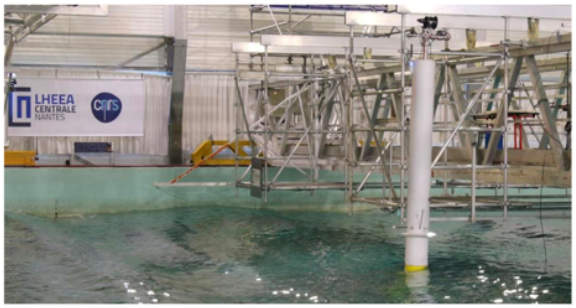

OPTIMISATION DE PALES D'HYDROLIENNE

OPTIMIZATION OF TIDAL TURBINE BLADES

M. Biçakli[1], N. Razaaly [2], L. Chatellier[2]
mickael.bicakli@univ-poitiers.fr ; nassim.razaaly@ensma.fr ; ludovic.chatellier@ensma.fr

[1] Institut Pprime, Université de Poitiers, Poitiers
[2] Institut Pprime, ISAE-ENSMA, Chasseneuil-du-Poitou

Résumé

L'objectif de ce travail est de réaliser l'optimisation géométrique de pales d'hydrolienne en utilisant une combinaison de simulations basse et haute fidélité. L'hydrolienne tripale à axe horizontal développée par l'IFREMER, est prise comme point de départ. Le processus d'optimisation vise à augmenter le coefficient de puissance C_P tout en réduisant le coefficient de poussée C_T. Pour ce faire, la distribution de l'angle de calage, de la corde et de l'épaisseur de la pale est modifiée. Tout d'abord, une approche basse fidélité, utilisant la BEMT, est employée. Des simulations de plus haute fidélité sont ensuite exécutées à l'aide de la méthode RANS avec le logiciel STAR-CCM+. Pour réduire le nombre de simulations, une optimisation basée sur des métamodèles (Surrogate-Based Optimization) est effectuée à l'aide d'un optimiseur développé en interne. Une méthode de krigeage hiérarchique est utilisée pour prendre en compte simultanément les données provenant des calculs BEMT et CFD.

Summary

The goal of this work is to carry out the geometric optimization of tidal turbine blades using a combination of low and high-fidelity simulations. A 3-bladed horizontal axis water turbine previously investigated by IFREMER is taken as a starting point. The optimization process aims to increase the power coefficient C_P while reducing the thrust coefficient C_T. To achieve this, the distribution along the blade of pitch angle, chord and thickness is modified. First, a computationally efficient low-fidelity approach using the Blade Element Momentum Theory (BEMT) method is employed. High-fidelity CFD simulations are then executed using the RANS method with **STAR-CCM+**. To reduce the number of steps, a Surrogate-Based Optimization (SBO) is conducted using an in-house optimizer. A hierarchical kriging method is used to simultaneously take into account data coming both from BEMT and CFD.

I – Introduction

Nowadays, the importance of renewable energy is beyond doubt. Renewable energy is considered a key solution for the ecological transition. Marine current, a natural and readily available source of energy, can be harnessed by devices like tidal turbines. These turbines convert the kinetic energy of the moving water into mechanical energy, ultimately converted into electricity. The shape of a turbine's blades determines its aerodynamic performance and, consequently, its efficiency. To enhance the performance of tidal turbines, blade shape optimization can be conducted. To perform this kind of optimization, many numerical tools can be employed, with various levels of fidelity. Depending on computational cost, numerical tools can be categorized into two groups : high-fidelity and low-fidelity approaches. High-fidelity approaches have higher computational cost (several hours of computation) but are considered more accurate. Methods such as LES, URANS, and RANS fall into this category. Low-fidelity tools are less time-consuming (a few seconds or minutes of computation) but may produce less reliable results. The choice of numerical methods significantly impacts the optimization process, which aims to achieve the desired objectives with minimal computational resources while maintaining confidence in the results. For this reason, a multi-fidelity optimization is carried out. Multi-fidelity optimization uses low-fidelity approaches to identify relevant designs and concentrates computational effort on the promising designs using high-fidelity models. In this study, BEMT serves as the low-fidelity model, while high-fidelity computations are performed using RANS. The optimization process aims to increase the power coefficient C_P such that $C_T(\mathbf{X}) < C_{T_{init}}$, where $\mathbf{X}$ is the design vector and $C_{T_{init}}$ is the initial geometry's thrust coefficient. The operating conditions are set as : λ (Tip Speed Ratio) = 4.0, TI (Turbulence Intensity) = 1.5 % and U_∞ (upstream velocity) = 1 $m.s^{-1}$.

II – Geometry of the turbine

A 3-bladed horizontal axis water turbine previously investigated by IFREMER ([9, 3]) is taken as a starting point. The radius of the rotor, denoted R, has a value of 362.0 mm. The hub radius, denoted R_{hub}, has a value of 55.0 mm. To perform 3D RANS simulations, only the hub and the blades of the device are considered (Figure 1). The geometry is based on 63-4XX NACA 6-digit profile series, with truncated trailing edge (Figure 2).

In this study, the blade is parameterized using twenty-three 2D profiles. Each of these profiles corresponds to a specific section of the blade along its spanwise direction (Figure 1). These 2D profiles are defined by 3 parameters : chord, thickness and pitch angle denoted θ (Figure 2). With this parameterization, a complete blade design is defined by twenty-three triplets. Therefore, the best design can be found by optimizing the distribution of these 3 parameters along the blade.

The root (the base where the blade connects to the hub) of the blade is a cylindrical section with a diameter of 21 mm. Details of the initial blade parameterization are given in Table 4.

III – BEMT

III – 1 Description of the method

The Blade Element Momentum Theory (BEMT) combines the Blade Element Theory (BET) and the Momentum Theory (MT). BEMT relies on dividing the stream tube passing through the rotor disc into annular sections. Consequently, the blade is also divided into different sections

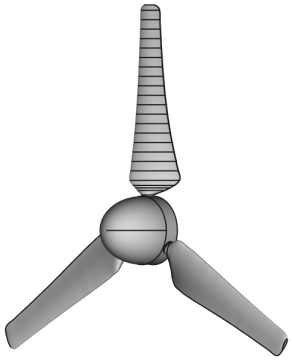

FIGURE 1 – Geometry of the hub and the blades, showing the different sections.

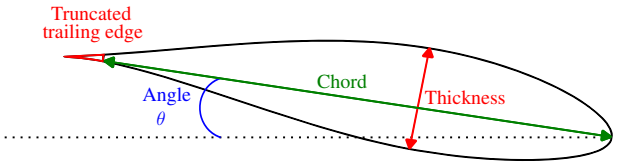

FIGURE 2 – Blade section parameterization.

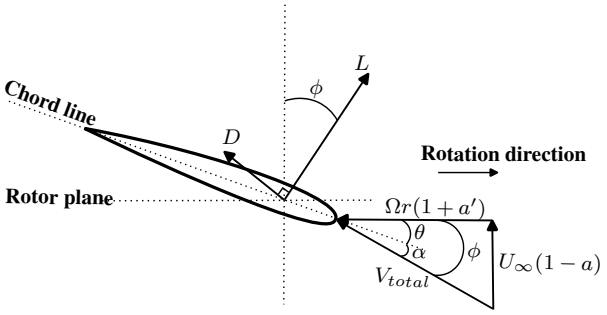

FIGURE 3 – Blade element section subjected to local velocity.

in the span-wise direction. On each of these sections, the momentum equation (Eq. 1) and the angular momentum equation are applied (Eq. 2).

$$dT_i = 4\pi r \rho U_\infty^2 (1-a) a F dr, \tag{1}$$

where dT_i is the thrust of the i^{th} element, r is the radius of the section, ρ is the water density, U_∞ is the upstream velocity, a is the axial induction factor, F is a correction factor to model the tip and/or hub loss and dr is the blade element and annular section width.

$$dQ_i = 4\pi r^3 \rho U_\infty \Omega (1-a) a' F dr, \tag{2}$$

where dQ_i is the torque of the i^{th} element, Ω is the rotation speed and a' is the tangential induction factor.

Within Blade Element Theory (BET), the thrust and torque are obtained by considering them as projections of the drag and lift forces acting on the blade element (Eq. 3 & 4). BEMT method leads to a nonlinear system of equations that can be solved to determine the axial and tangential induction factors.

$$dT_i = B\frac{1}{2}\rho V_{total}^2 (C_l \cos(\phi) + C_d \sin(\phi))\, c\, dr, \tag{3}$$

where B is the number of blades, $V_{total} = \sqrt{[U_\infty(1-a)]^2 + [\Omega r(1+a')]^2}$ is the total velocity at the section, C_l is the lift coefficient, C_d is the drag coefficient, ϕ is the relative flow angle and c is the chord of the profile.

$$dQ_i = B\frac{1}{2}\rho V_{total}^2 (C_l \sin(\phi) + C_d \cos(\phi))\, c\, dr \tag{4}$$

Power coefficient C_P and thrust coefficient C_T can be defined as follows :

$$C_P = \frac{Q\Omega}{\frac{1}{2}\rho\pi R^2 U_\infty^3}, \tag{5}$$

where Q is the total torque of the turbine, $Q = \sum_{i=1}^{N} dQ_i$ with i the section index and N the total number of sections.

$$C_T = \frac{T}{\frac{1}{2}\rho\pi R^2 U_\infty^2}, \tag{6}$$

where T is the total thrust of the turbine, $T = \sum_{i=1}^{N} dT_i$.

The polars of the different profiles are necessary to perform BEMT. Polars are generated using the software **XFOIL**. Polars are extrapolated using Viterna's method ([15]). N_{crit} parameter in **XFOIL** is utilized to predict the boundary layer transition from laminar to turbulent flow. N_{crit} can be determined with the following equation ([13]) :

$$N_{crit} = 5 - 6.18 \times \log^{10}(\text{TI}), \tag{7}$$

where TI is the turbulent intensity (in percentage) of the free-stream.

To perform the computation of the polars, **XFOIL** requires the Reynolds Number and the N_{crit} value. These parameters were set during the validation stage (section III – 2). There are numerous correction models for the BEMT to take account of hub and tip loss ([8]). These correction models are employed to improve BEMT prediction, involving modifications of the factor F in Eq. 1 & 2. In our study, various models were investigated. For tip loss, Glauert's model (Eq. 8) and Prandtl's model (Eq. 9) were evaluated.

$$F_{Glauert} = \frac{2}{\pi}\arccos\left[\exp\left(-\frac{B(R-r)}{2r\sin(\phi)}\right)\right], \tag{8}$$

where $F_{Glauert}$ is the Glauert's tip loss correction factor.

$$F_{Prandtl} = \frac{2}{\pi}\arccos\left[\exp\left(-\frac{B}{2}(1-\frac{\lambda_r}{\lambda})\sqrt{1+\lambda^2}\right)\right], \tag{9}$$

where $F_{Prandtl}$ is the Prandtl's tip loss correction factor and $\lambda_r = \dfrac{\lambda r}{R}$ is the local speed ratio.

For hub loss, AERODYN (NREL) model (Eq. 10) was evaluated.

$$F_{NREL} = \frac{B}{2}\frac{r - R_{hub}}{r\sin(\phi)}, \tag{10}$$

where F_{NREL} is a hub loss correction factor and R_{hub} is the hub radius.

If both hub loss and tip loss correction models are applied, the final correction factor F is obtained by multiplying the hub loss correction factor by the tip loss correction factor. If no correction is applied, the correction factor F is equal to one.

To select the model used during the optimization process, an investigation was conducted as part of the validation step (section III – 2).

III – 2 Validation

Experimental data, such as the evolution of the coefficients C_P and C_T as a function of TSR, are available for IFREMER's turbine geometry. These data were used for the validation step. In the present work, we performed the calibration of BEMT to improve the accuracy of its predictions. Four BEMT parameters were selected for calibration :

- Reynolds Number
- Turbulence Intensity (TI)
- Tip loss model
- Hub loss model

Different values were tested for each of these parameters. The aim of calibration is to find the combination of parameters that minimises the error between the experimental data and the BEMT predictions. The specific values tested for each parameter are listed in Table 2.

A Design of Experiment (DoE) was conducted to test every possible configuration of the parameters. To measure the quality of a configuration, a mean error is computed. This mean error is denoted σ_{BEMT} (Eq. 11). The performances observed experimentally and numerically are compared for the following TSR values : $\lambda = \{3.0,\ 3.5,\ 4.0,\ 4.5,\ 5.0\}$.

$$\sigma_{BEMT} = \frac{\sigma_{C_P-BEMT} + \sigma_{C_T-BEMT}}{2} \tag{11}$$

σ_{BEMT} is function of the mean error on C_P denoted σ_{C_P-BEMT} (Eq. 12) and of the mean error on C_T, denoted σ_{C_T-BEMT}.

$$\sigma_{C_P-BEMT} = \frac{1}{5}\sum_{i=0}^{4}\left|\frac{C_{P_{BEMT(i)}} - C_{P_{exp(i)}}}{C_{P_{exp(i)}}}\right|, \tag{12}$$

where i is the index of the different λ, $C_{P_{BEMT(i)}}$ is the power coefficient obtained for the i^{th} λ with the BEMT method and $C_{P_{exp(i)}}$ is the power coefficient obtained for the i^{th} λ experimentally.

σ_{C_T-BEMT} is obtained similarly to σ_{C_P-BEMT}, except that C_T is the quantity of interest instead of C_P. The configuration which minimises σ_{BEMT} is given in Table 1.

TABLE 1 – Optimal parameters for BEMT.

Reynolds	TI (%)	Tip loss model	Hub loss model
5.0×10^5	1.0	Glauert	No loss model

For this configuration $\sigma_{BEMT} = 11.6\ \%$. BEMT results with this configuration are shown in Figures 7. It can be seen that the accuracy of the BEMT method decreases as the TSR increases. This work focuses on optimizing for a fixed TSR value of 4.0. At this TSR, BEMT predictions for both C_P and C_T demonstrate good agreement with experimental data.

As previously indicated, the thickness distribution along the blade is optimized. This optimization process modifies the airfoil profile for each section of the blade. Consequently, to assess the performance of a turbine design, it is necessary to compute polars for each of the twenty-three sections. This method takes a few minutes to evaluate a single turbine design.

If the polars are already known, it takes only few seconds to perform BEMT for a full turbine geometry. Based on this observation, polars were computed for every thickness between 10 % and 60 % with a step of 0.5 %. Then, linear interpolation is achieved to compute polars. This technique significantly reduces computational cost.

The error caused by the interpolation is evaluated for the initial geometry. The mean error is denoted σ_{interp} (Eq.13). This error is function of the mean error on C_P denoted $\sigma_{C_P-interp}$ (Eq. 14) and of the mean error on C_T denoted $\sigma_{C_T-interp}$.

$$\sigma_{interp} = \frac{\sigma_{C_P-interp} + \sigma_{C_T-interp}}{2} \tag{13}$$

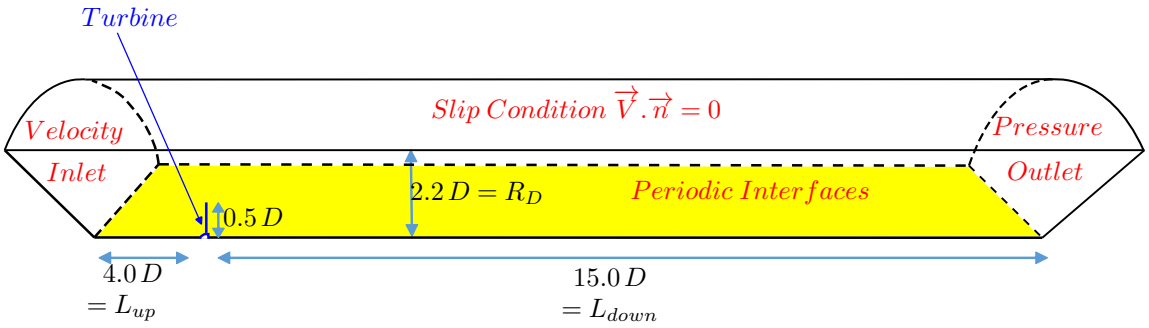

FIGURE 4 – Fluid domain and boundary conditions for RANS simulation.

$$\sigma_{C_P-interp} = \frac{1}{5}\sum_{i=0}^{4}\left|\frac{C_{P_{BEMT(i)}} - C_{P_{BEMT-interp(i)}}}{C_{P_{BEMT(i)}}}\right|, \tag{14}$$

where $C_{P_{BEMT-interp(i)}}$ is the power coefficient obtained for the i^{th} λ with the interpolated polars. The equation to calculate $\sigma_{C_T-interp}$ is similar to Eq. 14, except that C_P is not the quantity of interest ; it is C_T.

Finally, the mean error σ_{interp} caused by the interpolation for the initial geometry has a value of 0.12 %.

IV – RANS

IV – 1 Description of the method

Numerous studies ([16, 12]) have shown that RANS simulations provide good predictions of C_P and C_T at a lower computational cost compared to URANS or LES methods. That is why RANS simulations were conducted to assess the performance of the turbine. By exploiting the symmetry of the problem, only one third of the fluid domain and of the rotor are simulated. The result is a significant reduction in calculation time. A drawing of the fluid domain and of the boundary conditions is shown in Figure 4.

IFREMER's flume tank has a rectangular cross-section, with a width of $4\ m$ denoted W_{tank} and a height of $2\ m$ denoted H_{tank}. The radius R_D of the fluid domain has a value of $2.2\ D$, where $D = 0.724\,m$ is the diameter of the rotor. The value of R_D was chosen to maintain the observed blockage ratio in IFREMER's current flume tank. Indeed, the cross-sectional area of the fluid domain is equal to the cross-sectional area of IFREMER's tank (Eq. 15).

$$\pi R_D^2 = W_{Tank} \times H_{Tank} \tag{15}$$

The geometry of the turbine is generated with the open-source software **FreeCAD**. Meshing and CFD simulations are both conducted with the software **STAR-CCM+**.

IV – 2 Validation

To choose the upstream distance, denoted L_{up} and the downstream distance, denoted L_{down}, of the fluid domain, tests were conducted. It was verified that an increase in L_{up} or L_{down} does not modify the performance of the turbine.

The $k-\omega$ SST turbulence model is used for the study ([7]). RANS simulations can be achieved using a Single Reference Frame (SRF) method or by using Multiple Reference Frames (MRF). Tests were conducted with both methods. A better agreement with the experimental

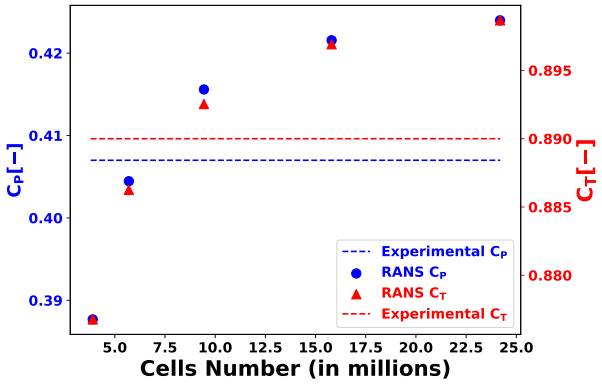

FIGURE 5 – Convergence study for C_P and C_T parameters, operating conditions : $\lambda = 4.0$, TI $= 1.5\ \%$, $U_\infty = 1\, m.s^{-1}$.

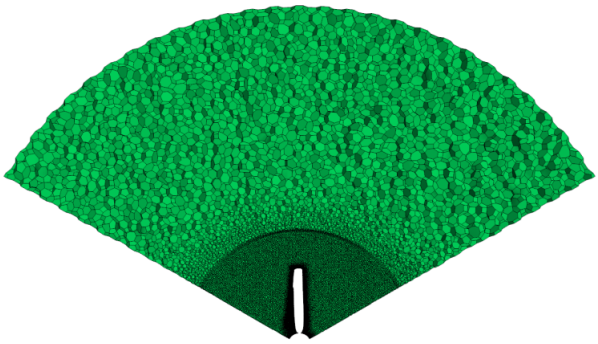

FIGURE 6 – Mesh of the cross-section of the fluid domain.

results and a reduction of the residuals errors was observed with MRF. For this reason this method was selected.

To select the mesh properties, simulations were carried out using polyhedral, tetrahedral, and trimmed meshes. Tetrahedral meshes were found to be unreliable due to repeatability issues. This means that even if two tetrahedral meshes are very similar, they could produce significantly different simulation results. Trimmed meshes and polyhedral meshes generated equivalent results in terms of C_P and C_T. However, trimmed meshes had the drawback of generating numerous poor quality cells at the trailing edge. Finally, the polyhedral meshes were preferred. To ensure a y^+ value lower than 1 on the blade, the near wall thickness of the prismatic layer was set to $2.4 \times 10^{-6}\, m$. Mesh refinement was applied near the blade and in the wake region. A view of the mesh in the cross-section is presented in Figure 6.

A convergence study was conducted on the initial geometry for both C_P and C_T parameters (Figure 5). The finest mesh used for the study is made of 24.2 million elements. Compared to the finest mesh, the 9.4 million elements mesh shows a difference of $2\ \%$ for C_P and of $0.7\ \%$ for C_T. During the optimization process, meshes are generated with the same configuration as the 9.4 million elements mesh.

Simulations were run on 96 CPUs, to reach convergence 4000 iterations were performed. The cluster used is composed of 16 Intel(R) Xeon(R) Gold 6252 CPUs, totaling 384 cores. Meshing is performed in parallel. Finally, the total computation time for a simulation with 9.4 million elements, including both meshing and CFD, is 1.2 hours. Key parameters are summarized in Table 3.

The validation step was completed for both BEMT and RANS computations, comparisons of these methods are presented in Figure 7.

V – Optimization method

V – 1 Modification of the blade

In order to reduce the dimension of the design vector, the distribution of chord, thickness and angle along the blade are parameterized using a method which combines B-splines and Free-Form Deformation (FFD) ([11]). A diagram illustrating the principle of the method is shown in Figure 8, a more detailed explanation is provided below. For each distribution, a regression is performed along the blade to determine the position of the B-spline's control points. On the diagram, the distribution used for the regression is represented by green triangles ("Data

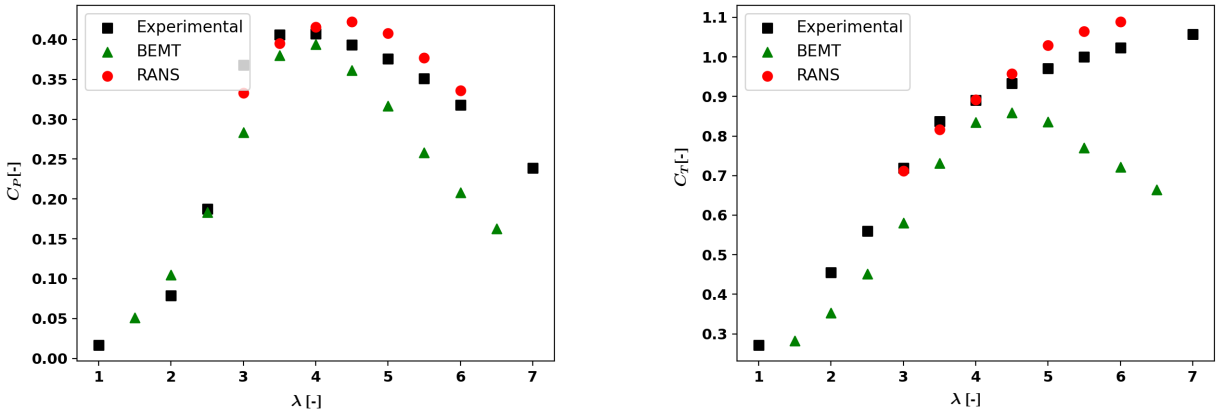

FIGURE 7 – Comparison of RANS and BEMT methods against experimental data for C_P (left) and C_T (right).

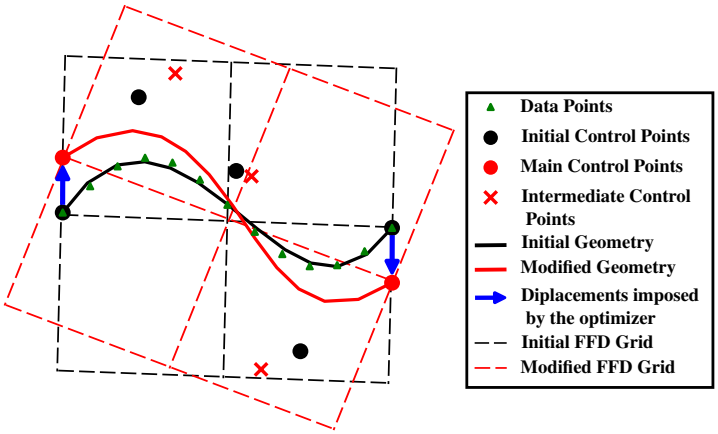

FIGURE 8 – Diagram of the parameterization using B-spline and FFD.

Points"). The initial B-spline obtained is represented by a black curve ("Initial Geometry") and has 5 control points ("Initial Control Points"). To create a new blade shape, these initial control points will be displaced in two ways : directly by the optimizer or by FFD method.

First, some selected control points are directly adjusted by the optimizer, as shown by the blue arrows in Figure 8. The new positions of those control points are represented by red dots, they are referred as "Main Control Points". An "Initial FFD Grid" is constructed based on the positions of the Main Control Points before their displacements. This grid is then deformed to create a "Modified FFD Grid" that reflects the new positions of the Main Control Points.

Next, the control points that were not directly displaced by the optimizer are moved using the FFD method. The new positions of these points are represented by red crosses and are referred to as "Intermediate Control Points".

The final B-spline, defined by the displaced control points (Main Control Points and Intermediate control Points), is highlighted in red in the diagram and is referred to as "Modified Geometry".

For chord, thickness and angle distributions, 4 control points are selected to be directly adjusted by the optimizer. Chord distribution is presented in Figure 10). This results in a design vector $\mathbf{X}$ of dimension 12. The vector is normalized, all its components are between -1.0 and 1.0.

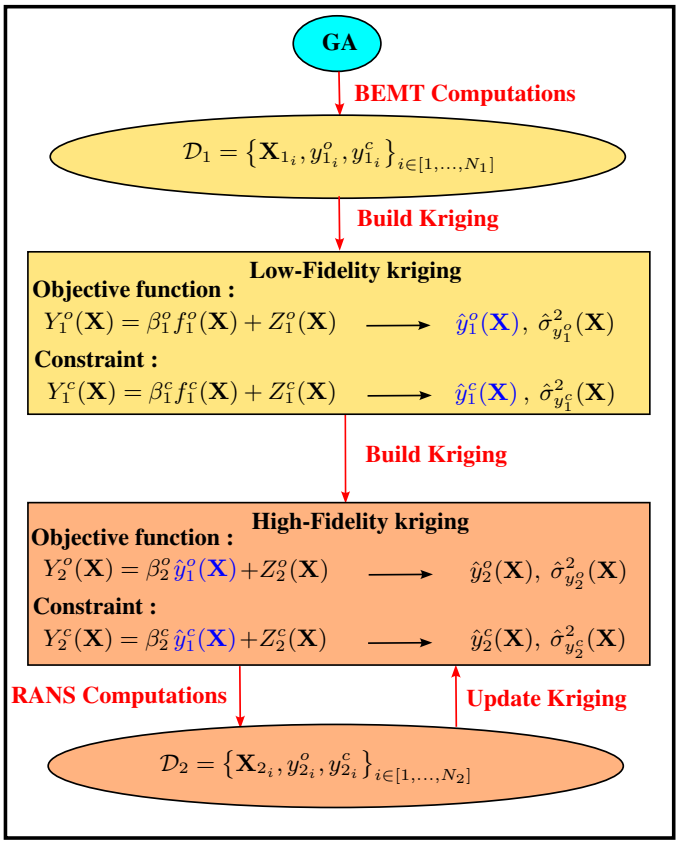

FIGURE 9 – Diagram of the optimization workflow.

V – 2 Multi-fidelity strategy : Hierarchical Kriging

The optimization process aims to increase the power coefficient C_P such that $C_T(\mathbf{X}) < C_{T_{init}}$, where $\mathbf{X}$ is the design vector and $C_{T_{init}}$ is the initial geometry's thrust coefficient. This optimization problem can be expressed as follows :

$$\begin{aligned} \text{Min} \quad & -C_P(\mathbf{X}) \\ \text{subject to} \quad & \\ & \mathbf{X} \in [-1,1]^{12} \\ & C_T(\mathbf{X}) < C_{T_{init}}, \end{aligned} \tag{16}$$

with $-C_P(\mathbf{X})$ the objective function and $C_T(\mathbf{X}) - C_{T_{init}}$ the constraint function for which a negative value is seek.

The main steps of the optimization are presented in Figure 9, explanations are given below. It is well known that Genetic Algorithms (GA) are suited for tidal turbine geometric optimization ([6]). GA has the advantage of avoiding local minima and converging toward the global minimum. However, GA requires several evaluations to converge and can therefore be computationally expensive. In our study, the BEMT is a cheap-to-evaluate method to obtain the quantities of interest C_P and C_T. That is why GA is used for the low-fidelity approach. The differential evolution method from SciPy's optimization toolbox ([14]) was used as the GA. The constraint in the GA is managed by a penalization method.

A first Design of Experiments (DoE), $\mathcal{D}_1$, is obtained with BEMT computations. $\mathcal{D}_1$ is generated by Latin Hypercube Sampling (LHS) ([5]). LHS is used to reduce discrepancy.

$\mathcal{D}_1 = \left\{\mathbf{X}_{1_i}, y^o_{1_i}, y^c_{1_i}\right\}_{i\in[1,\dots,N_1]}$, with $\mathbf{X}_{1_i}$ a design vector, $y^o_{1_i}$ a value obtained for the objective function, $y^c_{1_i}$ a value obtained for the constraint function and N_1 the size of the DoE. The index 1 refers to the low-fidelity approach, the index o to the objective function and c to the constraint.

$\mathcal{D}_1$ is then utilized to build kriging models corresponding to the low-fidelity method for both the objective function and the constraint function. The kriging method employed here is known as "Universal Kriging" (details in [4, 1]). With this method, it is assumed that the stationary random process for both the objective and the constraint functions has the following form :

$$Y(\mathbf{X}) = \beta f(\mathbf{X}) + Z(\mathbf{X}), \tag{17}$$

with β a vector to tune, f representing the trend functions, $Z(\mathbf{X})$ a stationary random process of null mean and covariance function given by $Cov[Z(\mathbf{X}), Z(\mathbf{X}')] = \sigma^2 R(\mathbf{X}, \mathbf{X}')$. σ^2 is the process variance, R the spatial correlation function depending on hyperparameters vector Θ and of the choice of a kernel. Here, a constant trend function $f : x \to 1$ and an exponential kernel are used. The hyperparameters are tuned by Maximum-Likelihood-Estimation ; further details can be found in references [4, 1].

The predictive means and variances for the low-fidelity kriging are denoted $\hat{y}^o_1,\ \hat{\sigma}^2_{y^o_1}(\mathbf{X})$ for the objective function and $\hat{y}^c_1(\mathbf{X}),\ \hat{\sigma}^2_{y^c_1}(\mathbf{X})$ for the constraint function.

Hierarchical kriging is used to build the kriging corresponding to the high-fidelity model. In fact, the predictive means of the low-fidelity kriging are used as trend functions for the high-fidelity kriging.

The predictive means and variances for the high-fidelity kriging model are denoted as $\hat{y}^o_2(\mathbf{X}),\ \hat{\sigma}^2_{y^o_2}(\mathbf{X})$ for the objective function and $\hat{y}^c_2(\mathbf{X}),\ \hat{\sigma}^2_{y^c_2}(\mathbf{X})$ for the constraint function. The means are utilized as surrogates, while the variances serve as error estimators for the predictions made by these surrogates.

To reduce the number of steps, a Surrogate-Based Optimization (SBO) is conducted using an in-house optimizer ([10]). SBO methods rely on cheap-to-evaluate surrogate models to approximate objective and constraint functions. During this process, new designs are tested with RANS simulations and the kriging is updated. The constraint is handled using a penalty term, resulting in a set of unconstrained minimization problems based on the surrogates.

VI – Preliminary results

The presented results are preliminary. An optimization process was conducted to test the method. The parameters for the low-fidelity approach are listed below :

- The differential evolution method from the SciPy library ([14]) was used as the GA with the following parameters : popsize = 15, maxiter = 10, polish = $True$.
- Total number of computations performed : 1992.

For the high-fidelity approach the parameters were :

- Number of computations for the initialization of the kriging (LHS) : 30
- Number of computations run in one loop : 5
- Number of loops : 4

A loop corresponds to a call of the optimizer, it is after each loop that the kriging is updated and new designs are given.

A total of 50 RANS simulations were conducted on a 96 CPUs cluster. The full optimization process with the high-fidelity approach took 65 hours to complete. The final distribution of the chord along the blade is presented in Figure 10. All the distributions are stored in Table 5.

Finally, by comparing the RANS results for both the initial and the optimized geometry, it can be seen that the optimized geometry increases C_P by 1.5 % and reduces C_T by 10.4 %.

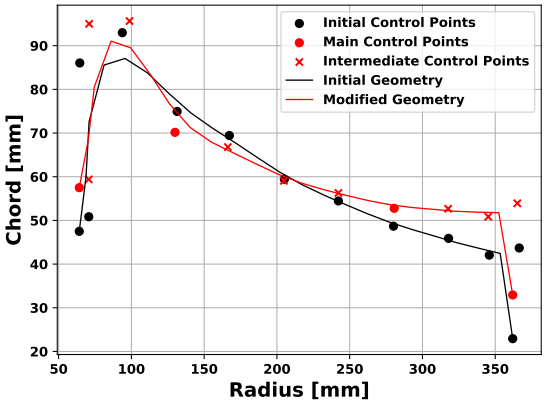

FIGURE 10 – Comparison of the chord distribution along the blade for nominal and optimized geometry.

VII – Conclusion

Geometric optimization of tidal turbine blades was conducted using a combination of low and high-fidelity simulations, yielding preliminary results. The method employs B-splines and Free-Form Deformation (FFD) to adjust the distribution of pitch angle, chord, and thickness along the blade. Initially, a computationally efficient low-fidelity approach based on Blade Element Momentum Theory (BEMT) is employed. Then, high-fidelity CFD simulations are executed using the RANS method. Surrogate-Based Optimization (SBO) is utilized to reduce computation time. Hierarchical Kriging (HK) is used to construct surrogates, enabling the use of low-fidelity kriging to construct a trend function for the kriging corresponding to the high-fidelity model. Validation of the numerical tools has been conducted to verify both the BEMT and RANS modeling against existing experimental results. Finally, the optimization process increases the power coefficient C_P by $1.5\ \%$ and reduces the thrust coefficient C_T by $10.4\ \%$.

References

[1] J.-M. Bourinet. *Reliability analysis and optimal design under uncertainty-Focus on adaptive surrogate-based approaches*. PhD thesis, Université Clermont Auvergne, 2018.

[2] M.-A. Dufour, G. Pinon, E. Rivoalen, F. Blondel, and G. Germain. Development and validation of a lifting-line code associated with the vortex particle method software dorothy. *Wind Energy*, 2024.

[3] B. Gaurier, C. Carlier, G. Germain, G. Pinon, and E. Rivoalen. Three tidal turbines in interaction : An experimental study of turbulence intensity effects on wakes and turbine performance. *Renewable Energy*, 148 :1150–1164, 2020.

[4] Z.-H. Han and S. Görtz. Hierarchical kriging model for variable-fidelity surrogate modeling. *AIAA journal*, 50(9) :1885–1896, 2012.

[5] J. C. Helton and F. J. Davis. Latin hypercube sampling and the propagation of uncertainty in analyses of complex systems. *Reliability Engineering & System Safety*, 81(1) :23–69, 2003.

[6] P. M. Kumar, J. Seo, W. Seok, S. H. Rhee, and A. Samad. Multi-fidelity optimization of blade thickness parameters for a horizontal axis tidal stream turbine. *Renewable energy*, 135 :277–287, 2019.

[7] F. R. Menter, M. Kuntz, R. Langtry, et al. Ten years of industrial experience with the sst turbulence model. *Turbulence, heat and mass transfer*, 4(1) :625–632, 2003.

[8] P. J. Moriarty and A. C. Hansen. Aerodyn theory manual. Technical report, National Renewable Energy Lab., Golden, CO (US), 2005.

[9] P. Mycek, B. Gaurier, G. Germain, G. Pinon, and E. Rivoalen. Experimental study of the turbulence intensity effects on marine current turbines behaviour. part i : One single turbine. *Renewable Energy*, 66 :729–746, 2014.

[10] N. Razaaly, G. Persico, and P. M. Congedo. Multi-fidelity surrogate-based optimization of transonic and supersonic axial turbine profiles. In *Turbo Expo : Power for Land, Sea, and Air*, volume 84089, page V02CT35A026. American Society of Mechanical Engineers, 2020.

[11] T. W. Sederberg and S. R. Parry. Free-form deformation of solid geometric models. In *Proceedings of the 13th annual conference on Computer graphics and interactive techniques*, pages 151–160, 1986.

[12] K. Thandayutham and A. Samad. Hydrostructural optimization of a marine current turbine through multi-fidelity numerical models. *Arabian Journal for Science and Engineering*, 45(2) :935–952, 2020.

[13] J. Van Ingen. The en method for transition prediction. historical review of work at tu delft. In *38th Fluid Dynamics Conference and Exhibit*, page 3830, 2008.

[14] P. Virtanen, R. Gommers, T. E. Oliphant, M. Haberland, T. Reddy, D. Cournapeau, E. Burovski, P. Peterson, W. Weckesser, J. Bright, et al. Scipy 1.0 : fundamental algorithms for scientific computing in python. *Nature methods*, 17(3) :261–272, 2020.

[15] L. A. Viterna and D. C. Janetzke. Theoretical and experimental power from large horizontal-axis wind turbines. Technical report, NASA Lewis Research Center, Cleveland, OH (United States), 1982.

[16] F.-w. Zhu, L. Ding, B. Huang, M. Bao, and J.-T. Liu. Blade design and optimization of a horizontal axis tidal turbine. *Ocean Engineering*, 195 :106652, 2020.

Acknowledgements

The authors acknowledge the IFREMER Centre Manche Mer du Nord for providing experimental data and information regarding the turbine geometry. Additionally, they acknowledge Laboratoire Ondes et Milieux Complexes (LOMC) located in Le Havre for generously providing access to their BEMT code ([2]).

Appendix

TABLE 2 – Parameter values for the BEMT validation.

Reynolds	**TI (%)**	**Tip loss model**	**Hub loss model**
1.0×10^4	1.0	Glauert	No loss model
5.8×10^4			
1.5×10^5	1.5		
1.7×10^5		Prandtl	AERODYN (NREL)
3.5×10^5	2.0		
5.0×10^5	3.0		

TABLE 3 – Summary of key parameters.

$R_D\,(m)$	$W_{tank}\,(m)$	$H_{tank}\,(m)$	$D\,(m)$
1.59	4.0	2.0	0.724
$L_{down}\,(m)$	**$L_{up}\,(m)$**	**Elements Number**	**Mesh**
10.9	2.9	9.4 million	Polyhedral
SRF/MRF	**TI (%)**	**Turbulence model**	**$U_\infty\,(m.s^{-1})$**
MRF	1.5	$k-\omega$ SST	1.0

TABLE 4 – Details of initial geometry blade profiles.

r/R	Chord (mm)	Thickness (%)	Pitch (deg)
0.152	21.0	*Cylinder*	*Cylinder*
0.157	21.0	*Cylinder*	*Cylinder*
0.177	47.50	43.0	23.2
0.189	60.00	32.0	22.8
0.200	72.26	27.0	21.8
0.222	87.50	22.0	20.7
0.264	86.59	21.3	17.3
0.306	83.30	21.4	14.2
0.348	79.06	21.7	11.9
0.390	74.94	22.0	9.9
0.432	71.10	22.2	8.4
0.474	67.55	22.4	6.9
0.515	64.20	22.5	5.8
0.557	61.20	22.5	4.9
0.599	58.40	22.4	4.1
0.641	55.79	22.2	3.3
0.683	53.52	21.9	3.0
0.725	51.48	21.5	2.3
0.767	49.63	20.9	2.0
0.809	47.95	20.2	1.4
0.851	46.38	19.5	1.1
0.893	44.98	18.6	0.7
0.934	43.65	18.0	0.3
0.976	42.45	18.0	0.2
1.000	22.93	25.0	-0.5

TABLE 5 – Details of optimized blade profiles.

r/R	Chord (mm)	Thickness (%)	Pitch (deg)
0.152	21.0	*Cylinder*	*Cylinder*
0.157	21.0	*Cylinder*	*Cylinder*
0.177	57.5	38.0	31.1
0.189	68.6	26.9	30.4
0.200	80.6	22.1	29.6
0.222	91.0	17.4	27.8
0.264	89.5	15.7	24.0
0.306	83.4	16.6	20.2
0.348	76.6	17.0	17.1
0.390	71.3	17.2	14.6
0.432	67.9	17.8	12.4
0.474	65.4	18.8	10.4
0.515	62.9	19.6	8.6
0.557	60.5	20.1	7.0
0.599	58.6	20.5	5.6
0.641	57.1	21.0	4.3
0.683	55.8	21.4	3.0
0.725	54.6	21.4	2.0
0.767	53.6	20.9	1.3
0.809	53.0	19.6	1.0
0.851	52.5	18.1	1.0
0.893	52.1	16.5	1.1
0.934	51.9	14.5	1.4
0.976	51.8	13.7	1.8
1.000	32.9	20.0	1.5